DOPPLER TOMOGRAPHY

T.R. MARSH

Department of Physics, University of Warwick, Coventry CV4 7AL, U.K.;
E-mail: t.r.marsh@warwick.ac.uk

(accepted April 2004)

Abstract. I review the method of Doppler tomography which is widely used to understand the complex emission line profile variations displayed by accreting binary stars. Doppler tomography uses the information encoded in line profiles as a function of orbital phase to calculate the strength of emission as a function of velocity, using a process closely related to medical X-ray tomographic imaging. I review applications which have revealed spiral structures in accretion discs, the accretion flows within magnetically-dominated systems and irradiation induced emission in X-ray binary stars. I also cover some of the more recent extensions to the method which variously allow for Roche geometry, modulation of the fluxes and motion at angles to the orbital plane.

Keywords: accretion

1. Introduction

The modeling of the light curves and spectra of binary stars has reached a high level of refinement. If one can understand the physics well enough, it is possible to produce a parameterised model, and then given data, compute the region of parameter space that it supports. While degeneracies are always a problem, the process is nevertheless familiar and well-understood. However, we cannot always apply this process with confidence. The structures of accreting binary stars are many and various, and very often we have little idea of how their brightness varies with position. Consider an accretion disc. We can perhaps assume that it is flat, just as we can assume a star to be spherical or tidally distorted (although a flat disc is not nearly as secure an approximation). The difficulty comes with the surface brightness. Stars have limb and gravity darkening and irradiation, which although not perfectly understood, are pillars of certainty compared to the surface brightness distribution over accretion discs. While parameterisation is still possible (e.g. a power law in radius), it can be misleading when there is no clear reason to suppose any particular pattern *a priori*. A power law in radius for instance can only fit axi-symmetric distributions. While one can add more complexity, it becomes hard to know what to add or when there is enough flexibility. This is especially the case in accreting systems where the usual χ^2 goodness-of-fit is compromised by the erratic variability called flickering – even a correct model may not fit perfectly.

An alternative approach, pioneered for cataclysmic variable stars by Keith Horne (Horne, 1985), is to create a model of almost complete flexibility. For instance, one

Astrophysics and Space Science **296:** 403–415, 2005.

can divide up a disc into thousands of small elements and seek to determine the surface brightness of all the elements. Given a fine enough grid, such a model can fit arbitrary brightness distributions, but it will also be highly degenerate. To cope with this, Horne (1985) introduced the crucial ingredient of a regularising function, picking the image of maximum entropy consistent with the data.

Doppler tomography grew from Horne's work, but applies to spectra rather than light-curves. The essential basis of the method is that information about the distribution of line emission is encoded in the emission lines of a system through Doppler shifting. The paper presenting the method (Marsh and Horne, 1988) has been cited by over 200 other papers, and Doppler tomography is now commonly applied to the interpretation of the spectra of accreting binary stars. Doppler tomography has been applied to all types of cataclysmic variables and low mass X-ray binaries and Algols. It has been reviewed by Marsh (2001) and more recently in a series of short papers by Morales-Rueda (2004), Richards (2004), Schwope et al. (2004), Steeghs (2004), and Vrtílek et al. (2004). In this review I will cover the method briefly, but focus more upon the main results of its application.

2. Fundamental Principles

Consider the schematic plot of Figure 1. This shows lines of equal radial velocity over a disc in a close binary, as seen from the perspective of an observer located to the right of the picture. Two orbital phases are shown to make the point that the pattern of equal radial velocity lines is fixed in the observer's frame rather than that of the binary. From the perspective of the rotating frame of the binary, the dipole-field-like pattern rotates with the observer. If Doppler shifting is the dominant broadening mechanism, all emission within a given region of more-or-less equal radial velocity will end up at one particular part of the line profile (see for instance Figure 1 of Marsh (1986) for how this forms the well-known double peaks from accretion discs). Hence spectra tell us the integrated flux over particular regions of

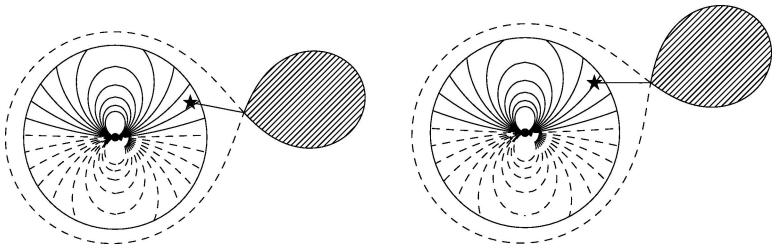

Figure 1. Schematic plots of a cataclysmic variable star, with the observer located off to the right of the images. Two orbital phases are shown, 0.03 (left) and 0.06. The filled circle is a white dwarf and the circle surrounding it is an accretion disc. Lines of equal line-of-sight speed are plotted. The solid lines are red-shifted, while the dashed lines are blue-shifted. The lines are stepped by $100\,\mathrm{km\,s^{-1}}$.

the disc. These regions continuously change orientation, and this can be used to obtain an image.

2.1. VELOCITY SPACE

Viewed in the spatial coordinates of Figure 1, the process of inverting data to obtain an image can seem complex. Things are a great deal simpler if viewed in terms of velocity coordinates. That is, instead of considering intensity as a function of (x, y, z) coordinates, we use (V_x, V_y, V_z) coordinates, where these are components of velocity as measured in an inertial frame that coincides with the rotating frame at orbital phase zero (the latter is usually defined by superior conjunction of the white dwarf when it is furthest from us). The coordinate axes are standardly defined by the direction from the white dwarf to the mass donor (x), the direction of motion of the mass donor (y) and the direction along the orbital axis (z), such that a right-handed set of axes is created. Figure 2 shows the equivalent of Figure 1, but now in velocity coordinates. Each structure plotted in Figure 1 has a well-defined velocity and can therefore be plotted in Figure 2. Take the mass donor for instance. We assume that it is co-rotating with the binary, and therefore is effectively in solid-body rotation with the binary, $\mathbf{v} = \omega \wedge \mathbf{r}$. This transform preserves the shape of the mass donor. Since it moves in the positive y-direction by definition, the mass donor ends up on the positive y axis. The important point about Figure 2 is that the dipole pattern of lines of equal radial velocity becomes a series of straight lines. Moreover, these lines can be plotted over all components, not just the disc. To do the same in Figure 1 would have required multiple sets of lines for the different components. I plot the stream twice in Figure 2: the lower curve, leading from the inner Langrangian point and ending with a star symbol to indicate the impact point with the disc, shows the velocity of the stream directly; the upper curve, also ending in a star, shows the velocity of

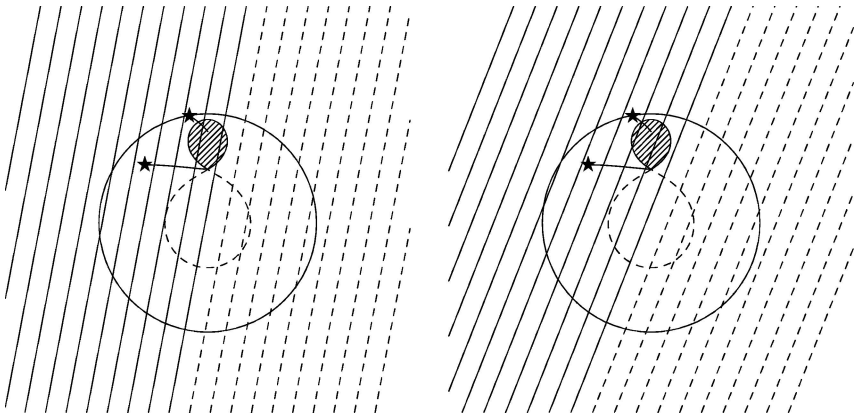

Figure 2. The equivalent of Figure 1 in terms of velocity coordinates.

the disc (assuming it has a Keplerian velocity field) along the path of the stream (somewhat unrealistically, since we don't expect the disc to extend as far as the inner Lagrangian point). There appears to be ambiguity here, however the ambiguity is felt most keenly if one attempts to reconstruct into *position* space, because spectra are measured directly in terms of velocity. Spots appear as sharp peaks which vary sinusoidally in velocity. Such a component can be assigned a unique position in velocity space, but when it comes to its position *we cannot say whether it might be directly from the stream or the disc along the stream without additional information*. This is a fundamental restriction which has lead me always to reconstruct in velocity space, despite starting from position space reconstructions in my thesis.

Provided that Doppler broadening dominates, all emission sources lying between two of the straight lines in Figure 2 will contribute to the same part of the emission line. Effectively the velocity space image is collapsed or 'projected' along the direction defined by these lines, which continuously alters as the binary rotates. A series of emission lines is thus equivalent to a series of projections at different angles of the same image. This is analogous to medical X-ray imaging in which we have a series of projections, measured by integrated optical depth to X-rays, of someone's head. This was a problem solved in the 1970s and goes back to work by Radon (1917). It goes under the name of 'Computerized Axial Tomography' (CAT scanning), or sometimes 'Computed Tomography' for short, and hence 'Doppler Tomography'.

2.2. Computing Doppler tomograms

There are two main methods used for implementing Doppler tomography. These have been described in some detail elsewhere (Marsh and Horne, 1988; Marsh, 2001), and so I will discuss them only briefly here. The main one presented by Marsh and Horne (1988) is based upon the same maximum entropy regularisation used by Horne (1985) in his 'eclipse mapping'. One divides velocity space into many elements and seeks the image of maximum entropy for a given goodness-of-fit measured with χ^2. This has the advantage of producing a model fit which can be compared directly with the data.

There is also a linear method which directly inverts the integrals defining the emission line formation by projection (the Radon transform). The usual method employed is that of 'filtered back-projection'. This is fast to compute, although speed is usually only an issue if hundreds of maps are being computed. Filtered back-projection is a two-step process in which first each spectrum is filtered. In Fourier space, the filter is proportional to $|k|$, where k is the wave number, and hence this filter enhances high frequencies. The second step is to compute

$$I(V_x, V_y) = \int_0^{0.5} f(\gamma - V_x \cos 2\pi\phi + V_y \sin 2\pi\phi, \phi)\, \mathrm{d}\phi, \tag{1}$$

where ϕ is the orbital phase, γ is the systemic velocity and $f(V, \phi)$ is the filtered profile as a function of velocity and orbital phase. This operation is known as 'back-projection,' because it can be viewed as smearing each profile along a direction defined by phase, which is almost the reverse of projection; see Marsh (2001) for details. One of the most useful aspects of the linear method is the intuition one gains from it in trying to understand artifacts. For example, a cosmic ray, if not removed, will lead to a streak across the image at an angle dependent upon the orbital phase of the spectrum affected. Small numbers of spectra also characteristically produce such structures. This is an obvious consequence of back-projection.

2.3. Principles of standard Doppler tomography

Doppler tomography allows for arbitrary brightness distributions, but not arbitrary data. A stationary component displaced from the systemic velocity γ for instance is impossible under the standard assumptions of Doppler tomography. These assumptions are as follows:

1. The visibility of all elements remains constant.
2. The flux of each element is constant.
3. Motion is parallel to the orbital plane.
4. All velocity vectors rotate with the binary.
5. The intrinsic width (e.g. thermal) of the profile is negligible.

It is item 4 which makes a stationary component displaced from γ an impossibility within standard Doppler tomography, for if such a component has velocity $\gamma + V$ at phase ϕ, it should have velocity $\gamma - V$ at phase $\phi + 0.5$.

It is *very common* for one or more of these assumptions to be wrong. A simple variation of emission line flux is one indication of possible problems. Item 1 is perhaps most commonly a problem. I will discuss later an attempt to deal with it. The result of such discrepancies are artifacts in the image. In the interpretation of Doppler tomograms one must always consider this possibility.

3. Applications of Doppler Tomography

In this section, I will review some of the applications of Doppler tomography, concentrating upon those which would have been difficult or perhaps impossible without it. Before looking at these maps some of which are complex, I show in Figure 3, a fairly simple example to illustrate some of the features shown by Doppler maps. The accretion disc produces a broad annulus. The *inner* edge of this annulus corresponds to the *outer* edge of the disc. Normally one does not expect emission from within the annulus except from the component stars. In the particular case shown there is emission from the (slowly rotating) white dwarf, which is not normally seen. As mentioned earlier, the mass donor is shown with its shape

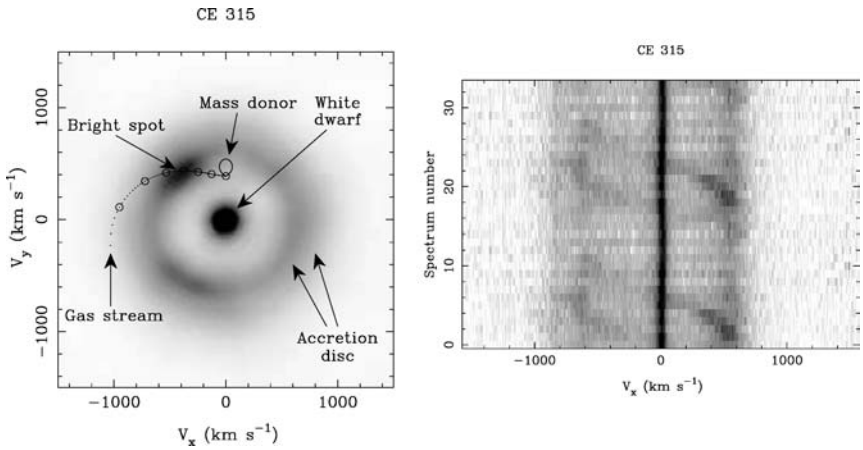

Figure 3. The left panel shows a Doppler map of the star CE 315 which shows many of the structures seen in Doppler images (labelled). The right panel shows the data (phase-folded). This system has an extreme mass ratio and thus the white dwarf is almost at the centre of mass at (0, 0). Both data and map are courtesy of Danny Steeghs.

preserved; we will soon see an example where emission is seen at its location. The gas stream however is not in solid-body rotation, and so is distorted compared to the usual shape in position coordinates. It is important to note that, whether or not distortion occurs, it is possible to make quantitative predictions for the position of any given component. The convention used in this figure is to mark radii along the gas stream by points every 0.01 (dots) and 0.1 (circles) of the inner Lagrangian distance, $R_{\rm L1}$. In this instance one can see that the gas stream hits the disc at $0.7R_{\rm L1}$, a measure of the radius of the disc.

3.1. RESULTS

I now go through a few key results from the application of Doppler tomography. I focus upon cataclysmic variables; the reviews mentioned in the introduction cover other types of systems.

3.1.1. *Spiral Structure*

The discovery of spiral structure in the dwarf nova IP Peg during outburst by Steeghs et al. (1997) is a key discovery only made possible by Doppler tomography. As shown in the left-hand panel of Figure 4, the profile changes in this system are complex and hard to interpret. This is caused by significant asymmetry in the brightness pattern, as can be seen in the centre panel, which shows the Doppler map computed from the data. Such structures were predicted in the 1980s to come from tidally driven shocks by Sawada et al. (1986) and Spruit (1987), and so this was the first interpretation of them (Steeghs et al., 1997). More recently, doubt has

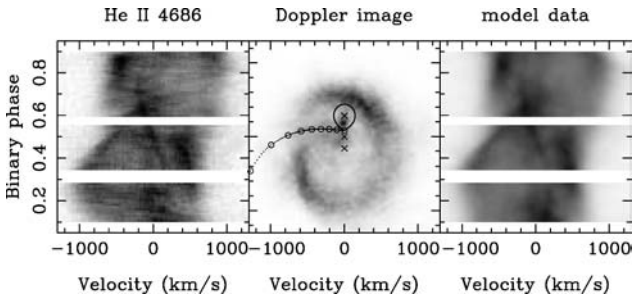

Figure 4. The figure shows trailed spectra (left), with time running upwards, of the dwarf nova IP Peg during outburst. The other panels show the Doppler image (middle) and the fit from the Doppler image (right). Figure taken from Harlaftis et al. (1999).

been cast upon the shock model (Ogilvie, 2002; Smak, 2001) with a combination of variable disc thickness and irradiation being the proposed alternative. As yet there is no clear solution to this problem.

3.1.2. *Emission from the Mass Donor in WZ Sge*

WZ Sge is a key object amongst cataclysmic variable stars. First of all, it is probably the closest of all CVs at only 43 pc (Thorstensen, 2003). It is also of interest for its very long inter-outburst period, which, until the most recent in 2001, was about 33 years. In July 2001, WZ Sge went into outburst only 23 years after its previous high state. Despite its closeness, WZ Sge remains a hard system to pin down, because its short orbital period (81.6 min) implies a very low mass and faint donor star, probably a brown dwarf. As a result, until 2001, the donor had never been detected. This changed during the outburst of 2001, when the donor showed line emission (Steeghs et al., 2001; see Figure 1) presumably as the result of irradiation during the outburst (Figure 5). The distance of the mass donor from the origin is a measure of its radial velocity semi-amplitude, which can be used to place a lower limit on the mass of the white dwarf. This turned out to be much larger than expected.

3.1.3. *Accretion Flows in Polars*

The accreting white dwarfs in some cataclysmic variable stars have magnetic fields strong enough to completely disrupt the accretion disc (surface field strength $\gtrsim$10 MG). These systems are known as polars. Although in these systems significant motion out of the orbital plane is expected, violating assumption 3 of Section 2.3, Doppler tomography has been applied to them with considerable success. Doppler images of polars have shown emission associated with the gas stream apparently before it is entrained into the magnetic field (the 'ballistic stream'), and also emission from the gas as it flows onto the magnetic poles Schwope et al. (2004).

These features were nicely brought out in the work of Heerlein et al. (1999) (Figure 6), who modelled the accretion in the polar HU Aqr. The problem of

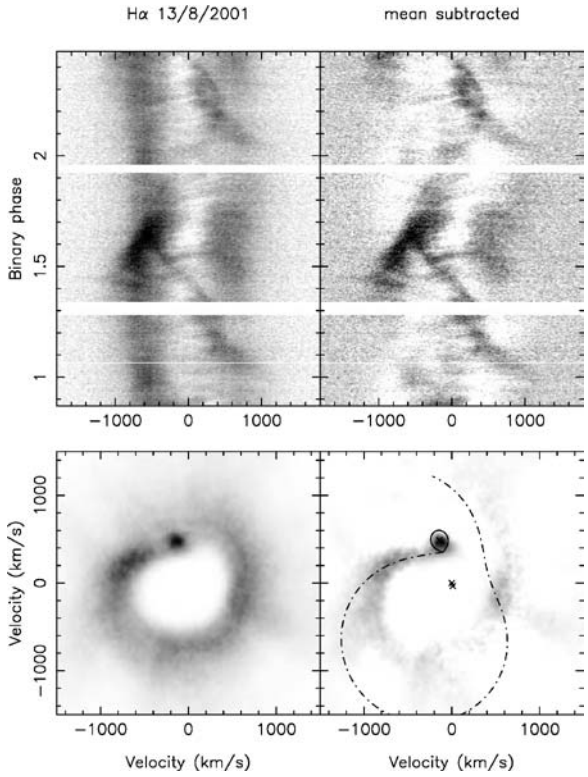

Figure 5. The data (top) and Doppler image (bottom) of WZ Sge taken during its July 2001 outburst. The right-hand panels show the same after subtraction of the symmetric part of the image and its equivalent from the data. Figure taken from Steeghs et al. (2001).

out-of-plane motion remains however. An attempt to account for this is described by Schwope et al. (2004).

3.1.4. *Bowen Fluorescence in Low-Mass X-ray Binary Stars*

The basic parameters of low-mass X-ray binaries (LMXBs) are notoriously difficult to pin down. The mass donor in particular is completely outshone by the accretion disc. It turns out, however, that the mass donors are sometimes visible in the light of the Bowen fluorescence lines near 4640 Å. This lead to the first detection of the mass donor in the famous system Sco X-1 (Steeghs and Casares, 2002). It is arguable whether Doppler tomography was necessary in this case, but it helped with the analysis, and can be invaluable in the case of low signal-to-noise ratios.

Doppler tomography has lead to similar discoveries in cataclysmic variables, and even signs of disc shadowing (Haralaftis et al., 1999; Morales-Rueda et al., 2000), which is seen in the tendency for irradiated emission to concentrate towards the poles of the mass donors. It has also been of great use for study of the gas stream/disc

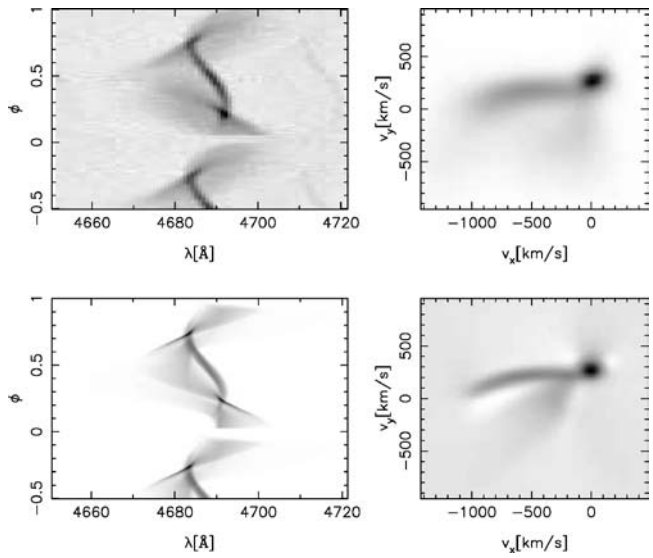

Figure 6. The spectra (top left) and Doppler image (top right) of the polar HU Aqr are plotted together with the equivalent pictures derived from a simple model of ballistic flow followed by magnetic entrainment (bottom panels). Figure taken from Heerlein et al. (1999).

impact in cataclysmic variable stars and black-hole binary stars (Marsh et al., 1990, 1994). Unfortunately there is not space to cover all of these areas, instead I turn to some of the ways in which Doppler tomography is being developed.

4. Extensions to Doppler Tomography

Since the presentation of Doppler tomography by Marsh and Horne (1988), several variations of the method have been presented. These can be split into two classes: those which add more physics, and those which allow for more flexibility. Bobinger et al. (1999) presented a combination of Doppler tomography and eclipse mapping, making use of a Keplerian velocity field to transform between space and position. Schwope et al. (2004) have started to work on simultaneous eclipse and Doppler mapping in polars, where they assume a curtain-like geometry for the magnetically-dominated flow. Both these fall into the first category of adding more physics. It remains to be seen how successful these extensions will be, but they can be criticised for adding additional assumptions, which are hard to be sure of. For instance, it is certainly *not* the case that the velocity field of all components is Keplerian, and the assumption that it is could lead to problems. There is however one case where the assumptions are fairly robust, which is the case of 'Roche tomography' (Rutten and Dhillon, 1994; Watson and Dhillon, 2001), in which the emission or absorption from the mass donor is mapped. The extra physics here is the shape and size of the Roche lobe, which are usually reasonably well constrained. The chief

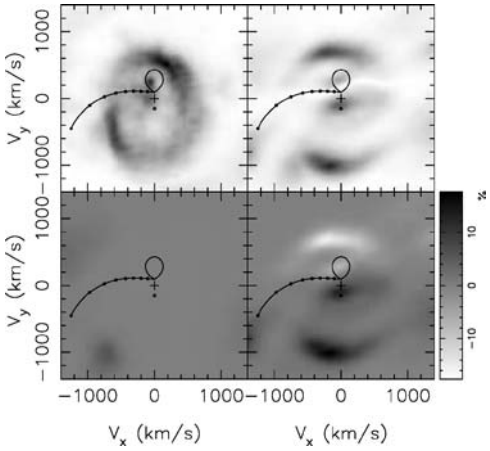

Figure 7. Doppler maps of IP Peg allowing for sinusoidal modulation (Steeghs, 2003). The top-left panel shows the average map (cf. Figure 4), while running clockwise from this are the amplitude of the modulation and the sine and cosine components.

difficulty in this case is obtaining data uncontaminated by emission from accretion flows.

The second approach of more flexibility has been pioneered by Billington (1995), who modelled spectra and eclipses with a fairly general velocity–position relation, and most recently by Steeghs (2003). The latter work allows for sinusoidal variation of the flux from each velocity with orbital phase, thus relaxing the first assumption listed in Section 2.3. This is a very generally applicable method, which Steeghs demonstrates leads to improved fits to data.

Interpretation of the results is tricky, but it does highlight regions of the images, which are likely to be affected by shadowing leading to modulation. For instance, Figure 7, which shows the modulation maps for IP Peg in outburst when spiral structure is present. There appears to be strong modulation close to the spiral arms, indicative of vertical structure causing shadowing.

4.1. Allowing for out-of-plane motion

As I have mentioned before, standard Doppler tomography does not allow for motion out of the orbital plane. Can it be modified to cope with this? The short answer is no, because it is possible to explain some line profiles as coming from a disc or equally well from a particular distribution of out-of-plane motion. This problem for example sometimes leads to an ambiguity between emission from a jet or a disc as an explanation for double-peaked emission. However, there are cases where one can deduce that there *must* be out-of-plane motion. I discussed earlier the case of a profile constantly offset from the systemic velocity as something that cannot be fitted using Doppler tomography, but it can easily be explained from

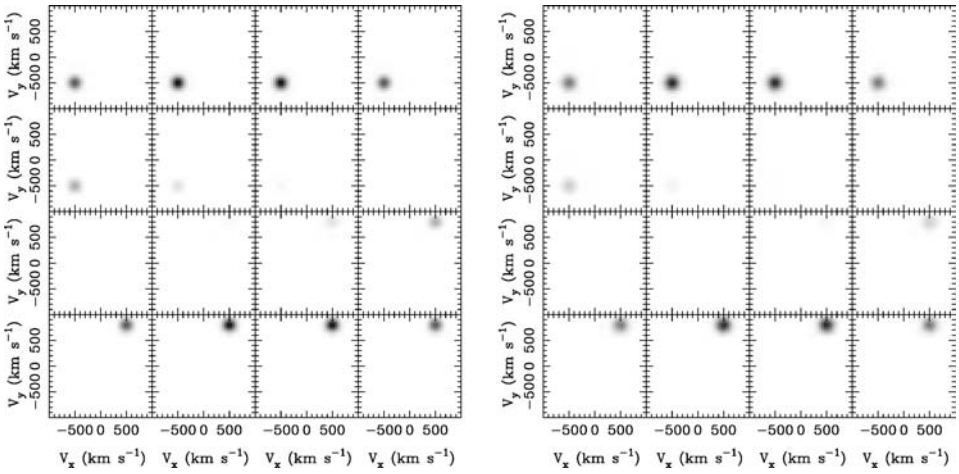

Figure 8. A model and reconstruction allowing for out-of-plane motion. The panels show slices of constant out-of-plane speed, V_z. The model consists of two spots located at $(-500, -500, -300)$ and $(+800, +500, +300)$ in units of km s^{-1}. The slices shown are stepped by 50 km s^{-1} in the V_z component and range from -375 (top-left) to $+375$ km s^{-1} (bottom-right).

out-of-plane motion. This suggests that there is some information on out-of-plane motion.

To test this I have carried out a reconstruction of data computed from a model, which includes out-of-plane motion, as shown in Figure 8. The reconstruction does appear to recover the out-of-plane motion. However, the fake data here had high signal-to-noise, and it is far from clear whether the reconstruction will survive lower signal-to-noise and especially a more realistic distribution of flux. Development of this method may however be useful as an indication of when out-of-plane motion is significant. Ultimately a more prescriptive technique such as that outlined by Schwope et al. (2004) might be preferable, if uncertainties of geometry can be controlled.

5. Observational Requirements for Doppler Tomography

Any review of Doppler tomography would be incomplete without some discussion of the data requirements for Doppler tomography. The key point to appreciate is that to create a map of a given resolution (e.g. 30 km s^{-1}) places requirements upon both spectral *and* time resolution. The time resolution must be such that features do not change their line-of-sight speed by more than the desired resolution during the exposure. For a feature of speed K from the centre of mass, the exposure time Δt must satisfy

$$\Delta t \lesssim \frac{P}{2\pi}\frac{\Delta V}{K}, \tag{2}$$

where ΔV is the velocity resolution desired. If we wish to cut ΔV by a factor 2, then we must cut Δt by the same factor, which would cut the number of photons per pixel by a factor of 4. It is thus very easy to become readout noise limited, even on a large telescope, and also to suffer from slow detector readout speed. Figure 3 is a good example of this: the data were taken with the echelle spectrograph UVES and the 8m VLT, and yet the resolution of the map is limited by the exposure time, which causes significant azimuthal smearing. Even at $V \approx 17.5$, which is bright by some standards, the target, CE 315, was too faint for the VLT and UVES given its orbital period of 65 mins and the high spectral resolution.

6. Conclusion

I have reviewed the method of Doppler tomography, which is now widely used in the interpretation of the spectra of binary stars. Doppler tomography has lead to the discovery of asymmetric structures in accretion discs and revealed details of the gas flow in a variety of types of systems, including magnetically-dominated binaries. There remain areas of both observation and analysis which can be improved. Data collection can be improved both in terms of resolution and time coverage. Analysis is often rather qualitative, and the issue of when a feature is real has rarely been tackled. With a wide range of applicability and much to improve, Doppler tomography will continue to be an essential analysis tool for binary stars for the foreseeable future.

Acknowledgements

I thank Keith Horne and Danny Steeghs for many conversations over the years and Danny for supplying the data for Figure 3. I thank PPARC for the support of a Senior Research Fellowship.

References

Billington, I.: 1995, *Images of Accretion Discs in Cataclysmic Variable Stars*.
Bobinger, A., Barwig, H., Fiedler, H., Mantel, K.H., Simic, D. and Wolf, S.: 1999, *A&A* **348**, 145–153.
Harlaftis, E.T., Steeghs, D., Horne, K., Martín, E. and Magazzú, A.: 1999, *MNRAS* **306**, 348–352.
Heerlein, C., Horne, K. and Schwope, A.D.: 1999, *MNRAS* **304**, 145–154.
Horne, K.: 1985, *MNRAS* **213**, 129–141.
Horne, K. and Marsh, T.R.: 1986, *MNRAS* **218**, 761–773.
Marsh, T.R.: 2001, Doppler Tomography. *LNP Vol. 573: Astrotomography, Indirect Imaging Methods in Observational Astronomy*, pp. 1–26.
Marsh, T.R. and Horne, K.: 1988, *MNRAS* **235**, 269–286.
Marsh, T.R., Horne, K., Schlegel, E.M., Honeycutt, R.K. and Kaitchuck, R.H.: 1990, *ApJ* **364**, 637–646.
Marsh, T.R., Robinson, E.L. and Wood, J.H.: 1994, *MNRAS* **266**, 137+.

Morales-Rueda, L.: 2004, *Astronomische Nachrichten* **325**, 193–196.
Morales-Rueda, L., Marsh, T.R. and Billington, I.: 2000, *MNRAS* **313**, 454–460.
Ogilvie, G.I.: 2002, *MNRAS* **330**, 937–949.
Potter, S.B., Romero-Colmenero, E., Watson, C.A., Buckley, D.A.H. and Phillips, A.: 2004, *MNRAS* **348**, 316–324.
Radon, J.: 1917, *Ber. Verh. Sächs. Akad. Wiss. Leipzig Math. Phys. K1* **69**, 262–277.
Richards, M.T.: 2004, *Astronomische Nachrichten* **325**, 229–232.
Rutten, R.G.M. and Dhillon, V.S.: 1994, *A&A*, **288**, 773–781.
Sawada, K., Matsuda, T. and Hachisu, I.: 1986, *MNRAS* **219**, 75–88.
Schwope, A.D., Catalán, M.S., Beuermann, K., Metzner, A., Smith, R.C. and Steeghs, D.: 2000, *MNRAS* **313**, 533–546.
Schwope, A.D., Mantel, K.H. and Horne, K.: 1997, *A&A* **319**, 894–908.
Schwope, A.D., Staude, A., Vogel, J. and Schwarz, R.: 2004, *Astronomische Nachrichten* **325**, 197–200.
Smak, J.I.: 2001, *Acta Astronomica* **51**, 279–293.
Spruit, H.C.: 1987, *A&A* **184**, 173–184.
Steeghs, D.: 2003, *MNRAS* **344**, 448–454.
Steeghs, D.: 2004, *Astronomische Nachrichten* **325**, 185–188.
Steeghs, D. and Casares, J.: 2002, *ApJ* **568**, 273–278.
Steeghs, D., Harlaftis, E.T. and Horne, K.: 1997, *MNRAS* **290**, L28–L32.
Steeghs, D., Marsh, T., Knigge, C., Maxted, P.F.L., Kuulkers, E. and Skidmore, W.: 2001, *ApJL* **562**, L145–L148.
Thorstensen, J.R.: 2003, *AJ* **126**, 3017–3029.
Vrtílek, S.D., Quaintrell, H., Boroson, B. and Shields, M.: 2004, *Astronomische Nachrichten* **325**, 209–212.
Watson, C.A. and Dhillon, V.S.: 2001, *MNRAS* **326**, 67–77.